Transport and Stability Analysis of Dilute Magnetized Accreting Flows

Tanim Islam

University of Virginia, Department of Astronomy

3 December 2007

Outline

Mechanics of Accretion

- Angular momentum must be transported **outwards**:

$$2\pi R^2 \langle T_{R\phi} \rangle + R\Omega(R)\dot{M} = R_{\text{in}}\Omega(R_{\text{in}})\dot{M}.$$

  Where $\langle T_{R\phi} \rangle > 0$ is the averaged angular momentum flux carried out by the turbulence, $\dot{M}$ is the mass inflow rate, and we impose a no-stress condition at the inner boundary.

- Energy generated through gravitational infall must be **radiated** or **transported**. A local model of energy transport (Balbus, 2004a):

$$\frac{1}{R}\frac{\partial}{\partial R} R \langle F_{ER} \rangle - \frac{\dot{M}}{2\pi R^2}\left(\frac{1}{\rho_0}\frac{\partial p_0}{\partial R}\right) = -Q_- - \langle T_{R\phi} \rangle \frac{\partial \Omega}{\partial \ln R}.$$

  Where $\langle F_{ER} \rangle$ is a rate of local turbulent heat flux and Q_- is a radiative dissipation rate.

Classical Accretion Disk

- optically thick and/or radiatively efficient – $Q_- \approx -\langle T_{R\phi} \rangle \frac{\partial \Omega}{\partial \ln R}$. Therefore $L_{\text{accretion}} \rightarrow GM\dot{M}/(2R_{\text{in}})$.
- Temperature in outer disk goes as $T_{\text{disk}} \propto R^{-3/4}$. Assuming blackbody, disk spectrum (see, e.g., Lynden-Bell (1969); Frank et al. (2002)):

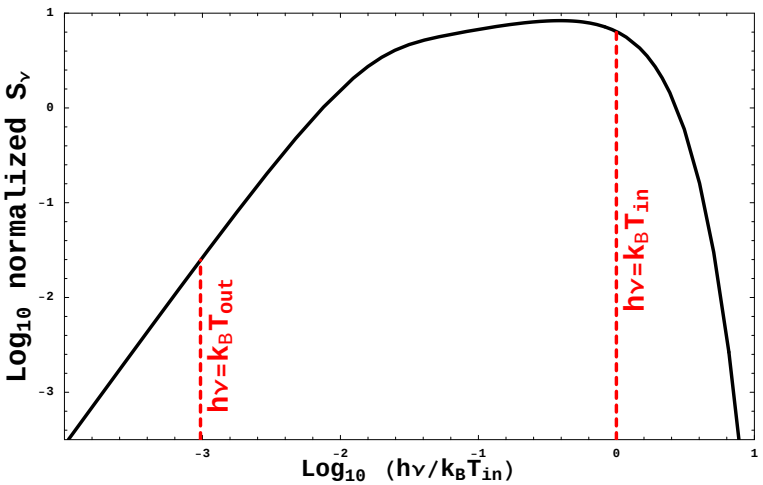

Normalized classical disk spectrum.

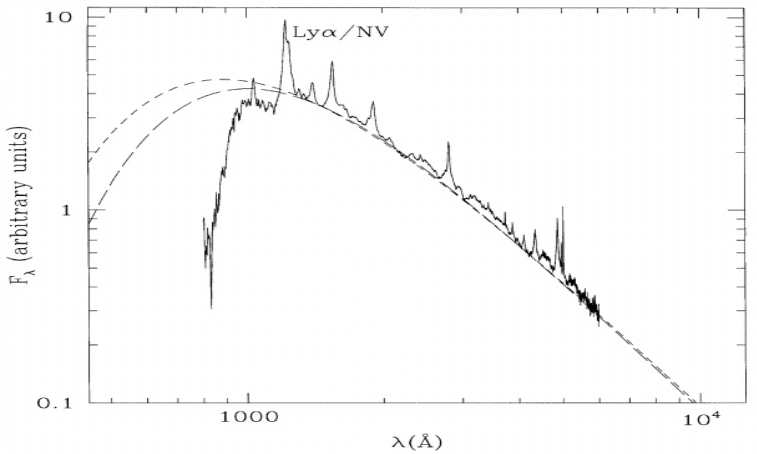

Fit of AGN "big blue bump" spectrum to classical disk blackbody. Figure is taken from Francis et al. (1991)

Insufficiency of Hydrodynamics

- Extremely high Reynolds numbers of astrophysical accretion flows led many to believe hydrodynamic turbulence as a source of angular momentum transport, but
- Hydrodynamic Keplerian flows are linearly stable.
  - numerical simulations (Balbus et al., 1996; Hawley et al., 1998; Lesur & Longaretti, 2005) demonstrate nonlinear stability and dissipation of initially random flows.
  - High-reynolds number hydrodynamic experiment (Ji et al., 2006) also demonstrates dynamically insignificant hydrodynamic turbulence and no angular momentum transport.

Insufficiency of Hydrodynamics

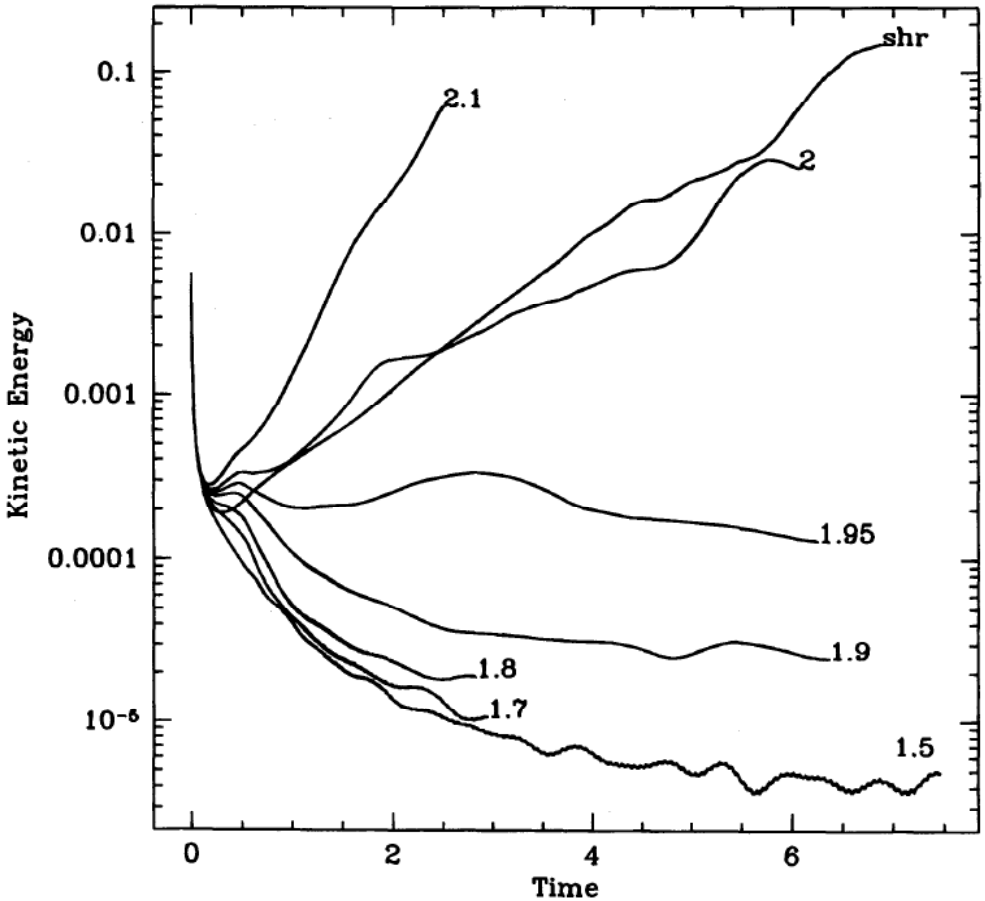

Only those simulations in which there is pure shear or in which $q = \partial \ln \Omega / \partial \ln R > 2$ demonstrate kinetic turbulence sustained against numerical dissipation. This figure is taken from Balbus et al. (1996).

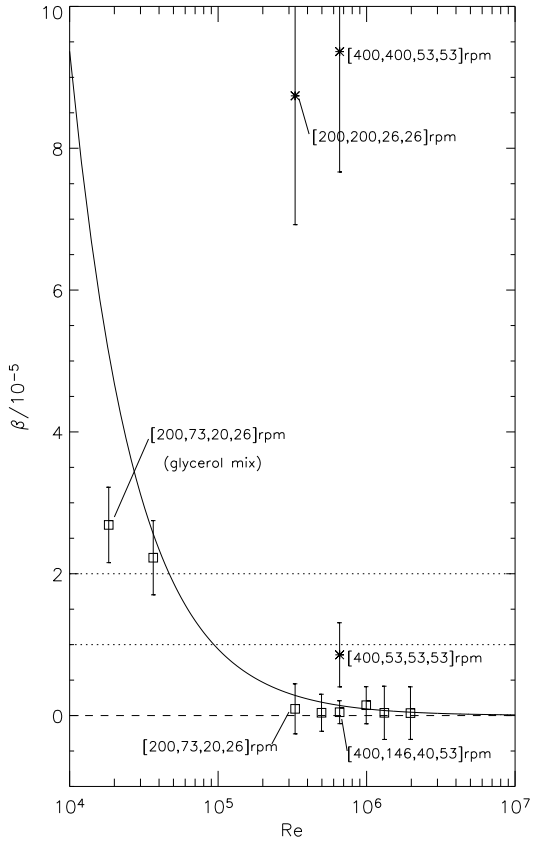

Angular momentum carried by the the Ji et al. (2006) Princeton Rayleigh-stable Taylor-Couette flow was found to be zero to within experimental errors for the highest Reynolds number trials.

The Magnetorotational Instability

- Velikhov (1959) and Chandrasekhar (1960) noted the linear instability of a metallic Taylor-Couette flow in which $d\Omega/dR < 0$, in the presence of arbitrarily small magnetic fields.
- Balbus & Hawley (1991) noted its promise in driving MHD turbulence that can allow accretion in a wide class of astrophysical systems.
- Observed in local and global numerical simulations, and in beginning experimental simulations of Rayleigh-stable Taylor-Couette metallic flows.

Cartoon Model of the MRI

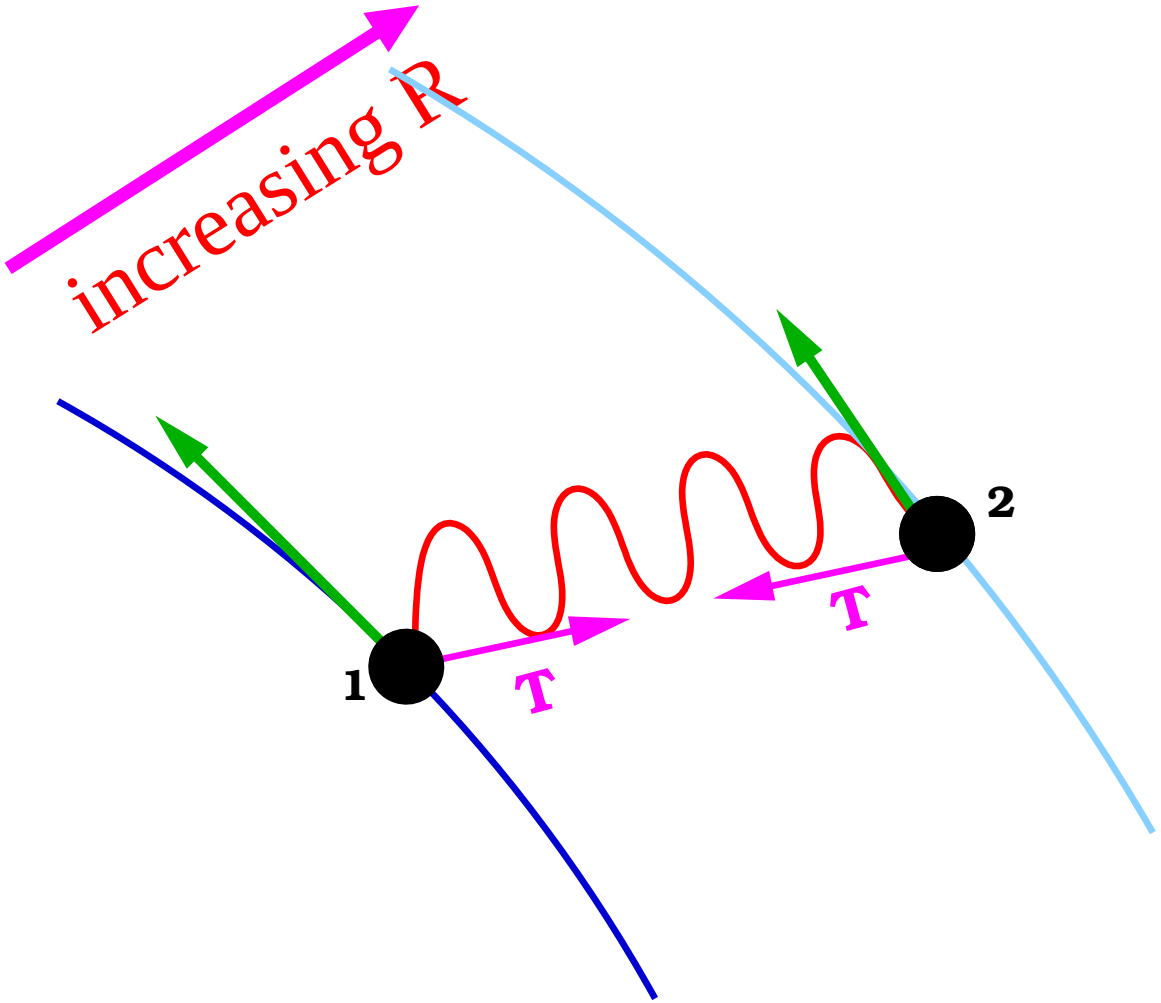

Tension provides a torque that speeds up the outer mass and slows down the inner mass. Angular momentum is transferred outwards, the spring tension increases, and the process runs away. Process ends when the tension is large enough that oscillation periods due to magnetic forces $\gtrsim$ orbital period.

Local Nonlinear Simulations

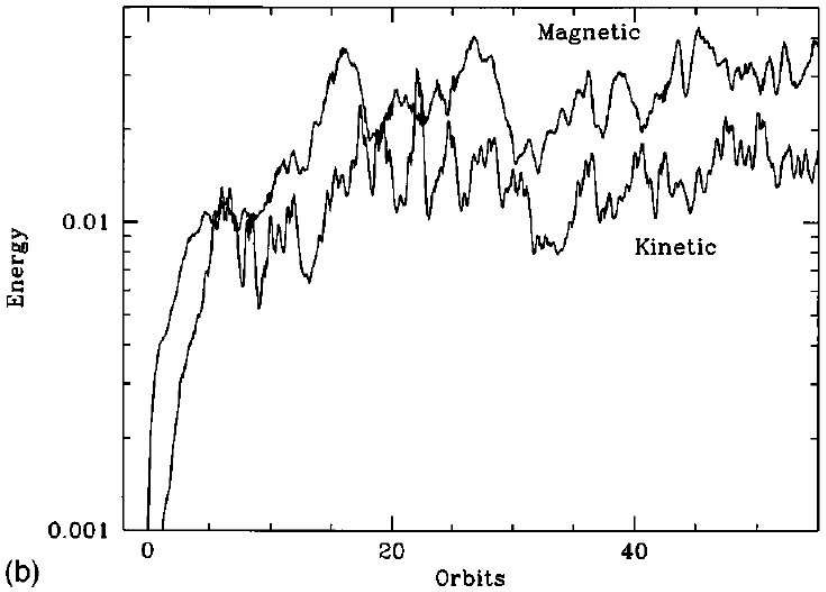

Saturation of magnetic and gas pressure fluctuations in a long-term shearing box simulation of a magnetized disk. This figure is taken from Hawley et al. (1996).

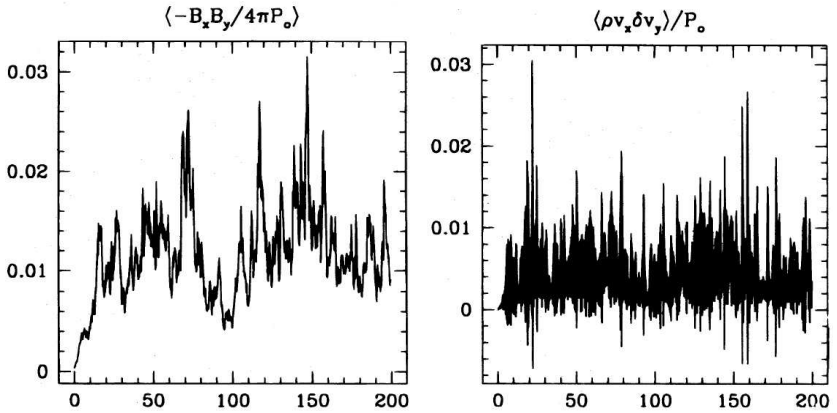

On the left is the evolution of the magnetic contribution, and on the right the kinetic contribution, to $\langle T_{R\phi} \rangle$. One can observe a net outwards flux of angular momentum associated with the nonlinear development of the MRI. The time is in units of orbital period. These figures are taken from Hawley et al. (1996).

Global Nonlinear Simulation

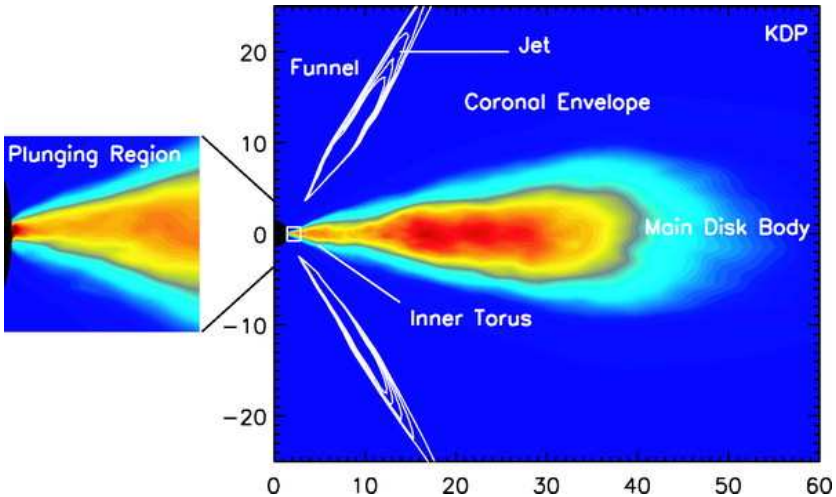

Azimuthally averaged density of a long time snapshot of a global MRI simulation of accretion onto a black hole, taken from De Villiers et al. (2003). These global simulations have the following features:

- relatively slender disks (thermal velocities $\lesssim$ orbital velocities)
- outlying coronal region of dilute, magnetic pressure dominated plasma
- centrifugally evacuated funnel region about rotation axis.

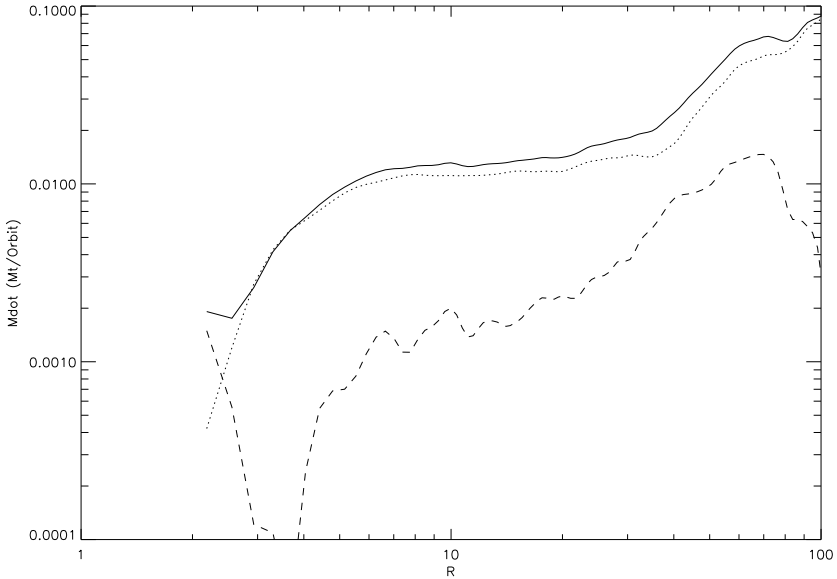

Time averaged mass accretion and outflow rates in initial global simulations of the MRI (Hawley et al., 2001). Accretion rates are low, the mass accretion and outflow rates decreases with decreasing radius down to the marginally stable orbit.

Characteristics of RIAFs

- At the current epoch, classical or radiatively efficient accretion onto central galactic black holes is relatively rare.
- Likely that most forms of accretion onto central galactic black holes are RIAFs (radiatively inefficient accretion flows)
  - very little gravitational energy is radiated, and optically thin.
  - Two-temperature nature of plasma in primary emitting regions – ions remain virial and adiabatic, electrons much cooler.
  - Dilute: ion mean free path of order or much larger than system scale.

Commonality of RIAFs?

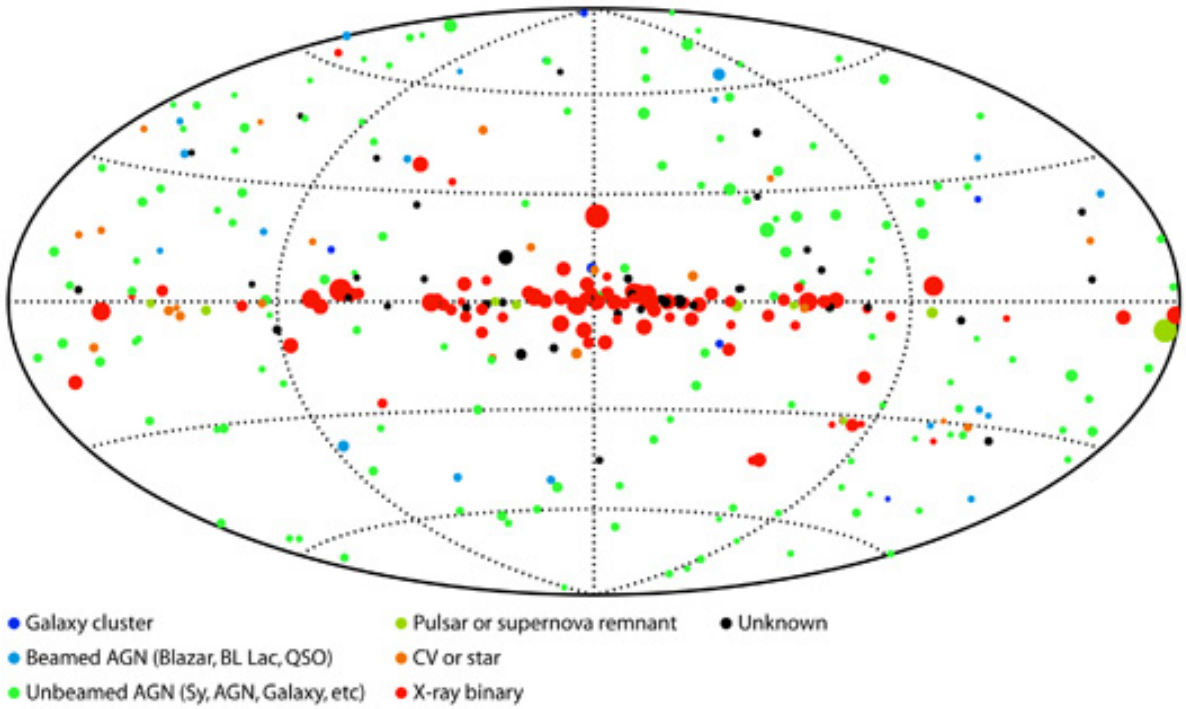

Complete survey of AGNs and quasars within the nearest 4×10^8 ly within Earth, taken with the SWIFT X-ray probe, taken from Winter et al. (2007). There exist only $\sim$ 200 instances of high-energy accretion onto supermassive central galactic black holes. This is only a few percent of total number of central galactic black holes (Richstone et al., 1998).

Underluminosity of RIAFs

Accretion Flow and X-Ray Luminosities of Dim Galactic Black Holes

Galaxy	d (Mpc)	M_{BH} ($\times 10^8 M_\odot$)	$R_{capture}$ (arcsec)	$L_{capture}$ (erg s^{-1})	L_X (erg s^{-1})
NGC 1399[1]	20.5	10.6	0.36	2.3×10^{44}	$\lesssim 9.7 \times 10^{38}$
NGC 4472[1]	16.7	5.65	0.24	4.5×10^{43}	$\lesssim 6.4 \times 10^{38}$
NGC 4636[1]	15.0	0.791	0.049	4.5×10^{41}	$\lesssim 2.7 \times 10^{38}$
M 82[2]	18.4	30	2	5×10^{44}	$\sim 7 \times 10^{40}$
Sag. A*[3]	8.5×10^{-3}	0.026[4]	2.2	6×10^{40}	2.2×10^{33}

[a] Taken from Loewenstein et al. (2001)
[b] Taken from Di Matteo et al. (2003)
[c] Taken from Baganoff et al. (2003)
[d] Mass measurement of Sag. A* taken from Schödel et al. (2002); Ghez et al. (2003)

Dilute Nature of RIAF Plasma

Dilute Nature of Dim Accreting Galactic Black Holes (table taken from Menou (2005))

Galaxy	$n(1'')$ (cm^{-3})	$T(1'')$ $(10^7\ \mathrm{K})$	$R(1'')$ (cm)	$\lambda(1'')/R(1'')$	$\lambda(1'')/R_{\mathrm{capture}}$
Sag. A*[1]	100	2.3	1.3×10^{17}	0.4	0.4
NGC 1399[2]	0.3	0.9	3.1×10^{20}	0.009	0.02
NGC 4472[2]	0.2	0.9	2.5×10^{20}	0.016	0.07
NGC 4636[2]	0.07	0.7	2.2×10^{20}	0.032	0.6
M 82[3]	0.17	0.9	2.7×10^{20}	0.018	0.02
M 32[4]	0.07	0.4	1.2×10^{19}	0.2	1.3

[a] Taken from Baganoff et al. (2003)
[b] Taken from Baganoff et al. (2003)
[c] Taken from Di Matteo et al. (2003)
[d] Taken from Ho et al. (2003)

Sagittarius A*

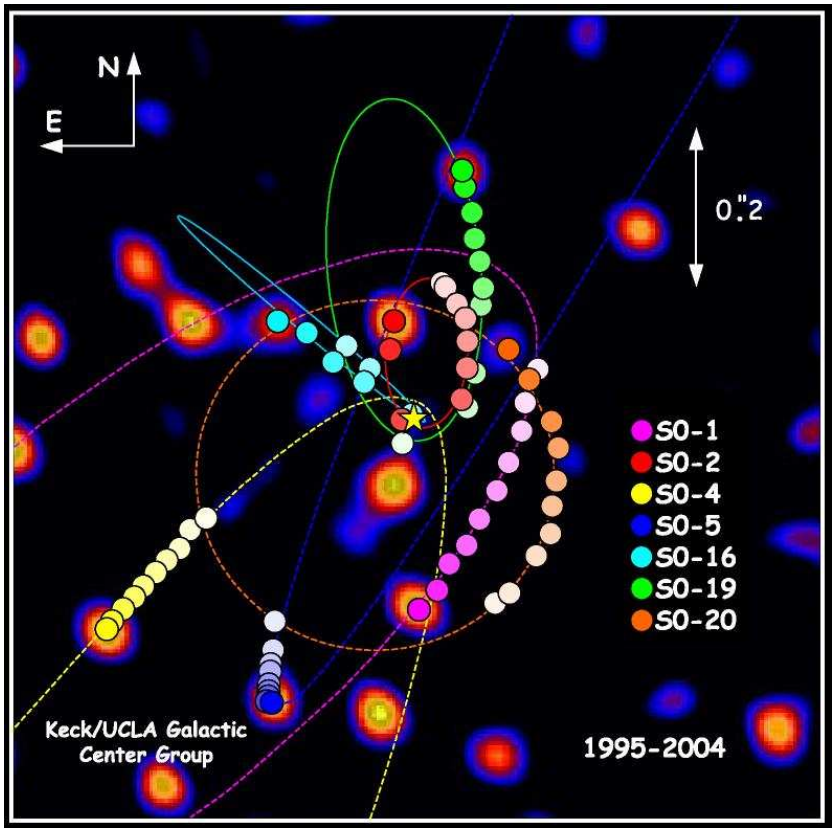

Time resolved orbits of stars orbiting Sagittarius A*, taken from http://www.astro.ucla.edu/∼ghezgroup/gc.

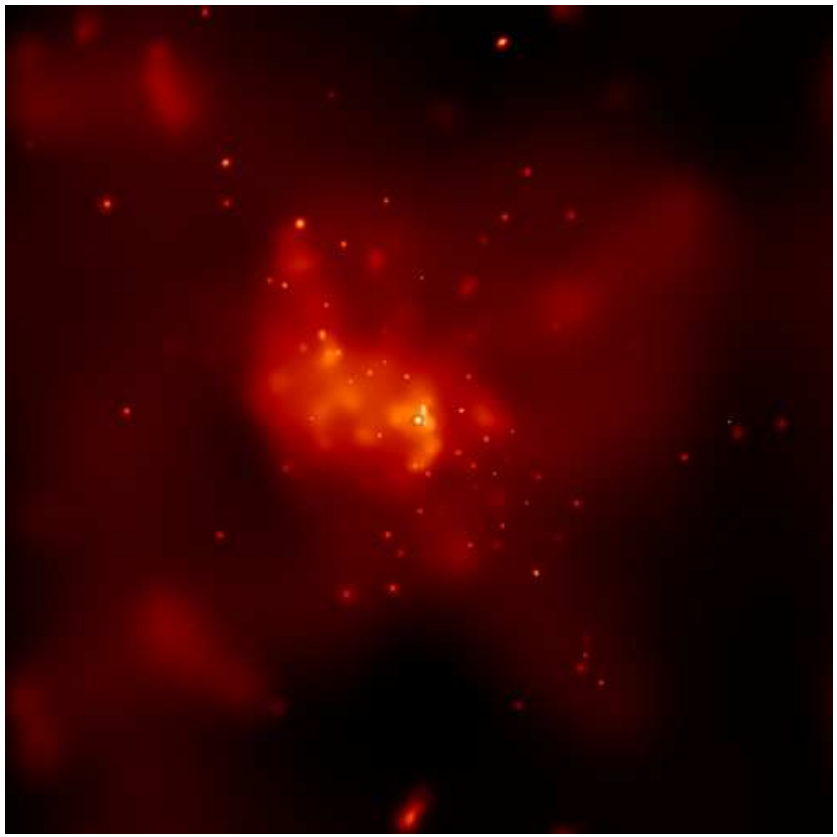

False color Chandra X-ray image of the 2-10 keV emission within 2 pc of the central galactic black hole Sagittarius A*. Image source is http://chandra.harvard.edu/photo.

Extreme Underluminosity of Sagittarius A*

- ambient conditions from Chandra X-ray data (Baganoff et al., 2003) imply $L_{\text{capture}} \sim 6 \times 10^{40}$ erg s^{-1}.
- Bolometric luminosity $L \sim 6 \times 10^{36}$ erg s^{-1} $\ll L_{\text{capture}}$ (Beckert et al., 1996; Narayan et al., 1998).
- Spectrum of Sag. A* not a good fit for efficient accretion.

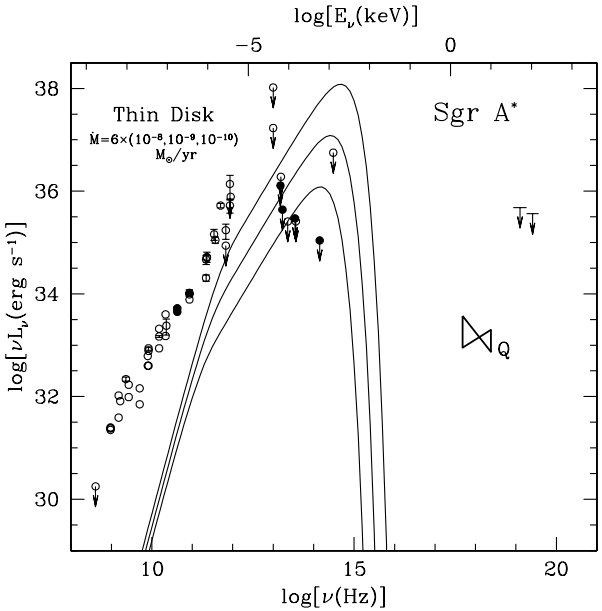

Poor spectral fits of Sag. A* bolometric emission to classical accretion disk spectrum at various mass accretion rates. This figure is taken from Narayan (2002).

Magnetic Fields About Sagittarius A*

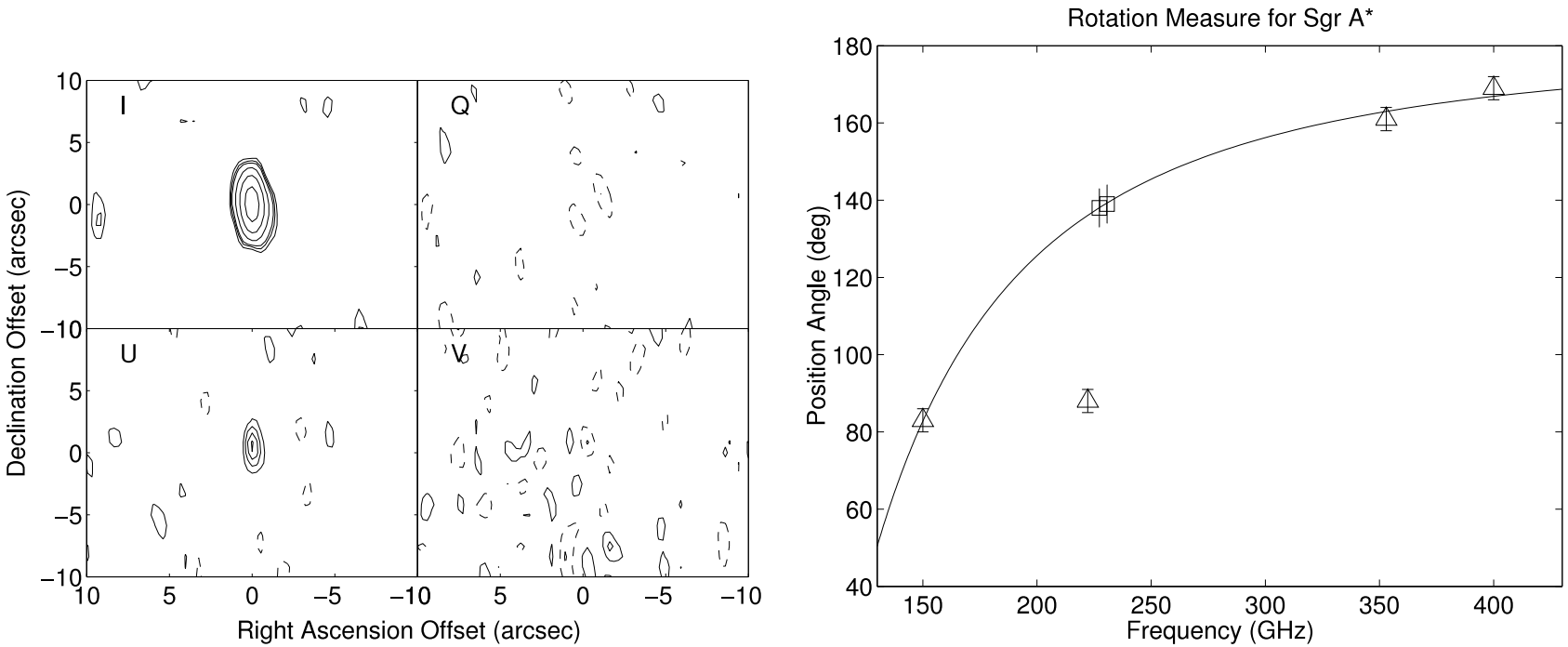

Evidence of internal magnetic field in Sag. A* from Faraday polarization at high radio frequencies. On the left is the unresolved 1'' millimeter and far infrared radio emission from the Sag. A* sources. On the right is difference between left and right circularly polarized radiation from Sag. A* as a function of frequency; the best-fit rotation measure $RM = 4.3 \pm 0.1 \times 10^{5}$ rad m^{-2}. This plot is taken from Bower et al. (2003).

In dilute plasmas in which ion cyclotron frequency $\gg$ inverse time scales of our problem of interest (such as collision frequency), momentum and energy transport become anisotropic and may become dynamically important.

- Heat flux and viscous stress tensor are modified:

$$\text{heat flux:} \qquad \mathbf{q} = q\mathbf{b}$$

$$\text{viscous stress tensor:} \qquad \boldsymbol{\sigma} = \sigma_{\mathbf{bb}} \left(\mathbf{bb} - \frac{1}{3}\mathbb{I} \right)$$

- The magnetothermal instability (MTI) transports thermal energy via magnetic-field-directed thermal flux where temperature decreases upwards/outwards (Balbus, 2001).
- The magnetoviscous instability (MVI) transports angular momentum outwards, via magnetic-field directed viscous stresses, when angular velocity decreases outwards (Balbus, 2004b; Islam & Balbus, 2005).

Magnetothermal Instability

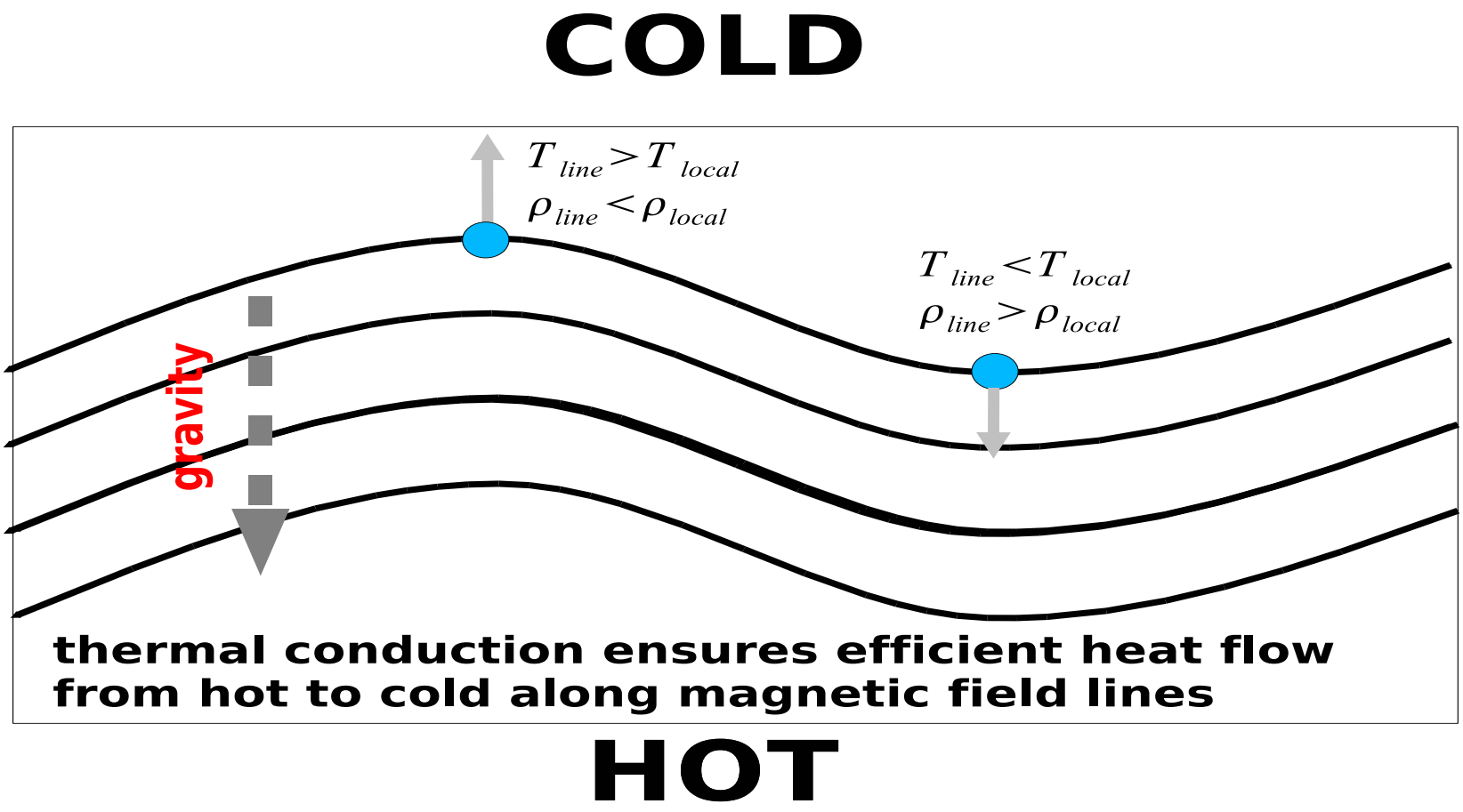

Magnetoviscous Instability

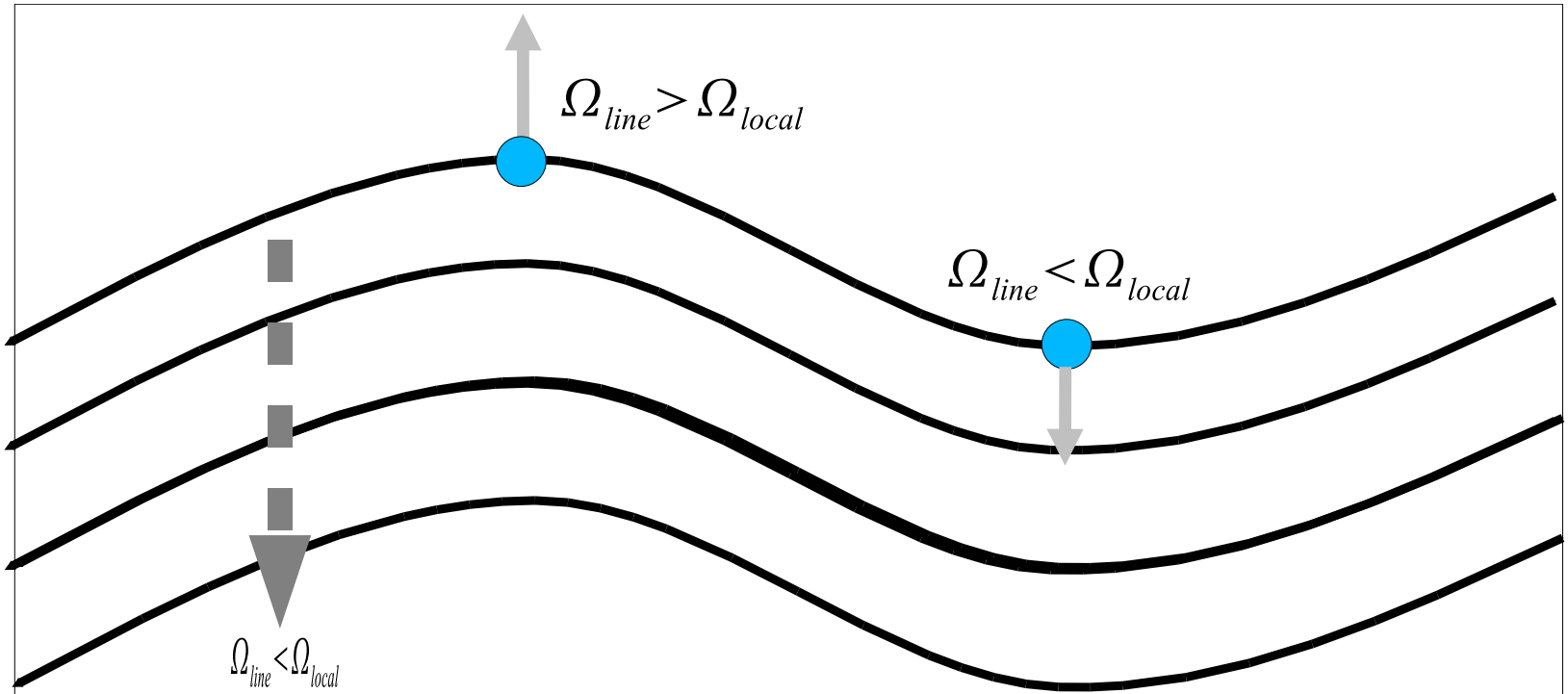

viscosity ensures efficient flow of angular velocity from the inner to outer point

Mechanics of Accretion in Dilute RIAF Disks

- For dilute, radiatively inefficient flows, turbulence must carry out both *angular momentum* and *thermal energy*:

$$2\pi R^2 \langle T_{R\phi} \rangle + R\Omega(R)\dot{M} = R_{\rm in}\Omega\left(R_{\rm in}\right)\dot{M}$$

$$\frac{1}{R}\frac{\partial}{\partial R}R\langle F_{ER}\rangle - \frac{\dot{M}}{2\pi R^2}\left(\frac{1}{\rho_0}\frac{\partial p_0}{\partial R}\right) = -\frac{\partial\Omega}{\partial \ln R}\langle T_{R\phi}\rangle$$

- **Angular momentum flux**:
$\langle T_{R\phi}\rangle = \left\langle \rho_0 \delta u_R \delta u_\phi - \frac{\delta B_R \delta B_\phi}{4\pi} + \delta\sigma_{\mathbf{bb}}\delta b_R b_{\phi 0}\right\rangle.$
- **Radial heat flux**:
$\langle F_{ER}\rangle = \left\langle \frac{5}{2}\rho_0\delta\theta\delta u_R + \delta q \delta b_R - \frac{1}{3}\delta\sigma_{\mathbf{bb}}\delta u_R\right\rangle.$

Equilibrium Disk Structure

- Plasma dynamics is considered in a rotating, cylindrical frame centered about the origin.
- Thin disk: $\Omega(R)^2 \approx GM/R^3$; isothermal sound speed $\theta_0 = p_0/\rho_0 \ll R^2\Omega(R)^2$.
- Equilibrium nonradial magnetic field, $\mathbf{B}_0 = B_0\left(\hat{\phi}\cos\chi + \hat{\boldsymbol{z}}\sin\chi\right)$.
- Isotherms along magnetic field lines, $T_0 \equiv T_0(R)$.
- Equilibrium profiles of temperature and pressure,

$$\alpha_T = -H\frac{\partial \ln T_0}{\partial R}, \quad \alpha_P = -H\frac{\partial \ln p_0}{\partial R}, \quad H = \sqrt{\frac{p_0/\rho_0}{GM/R^3}}.$$

Stability Analysis

- Examine axisymmetric nonradial modes, $\delta a \propto \exp\left(ik_Z z + \Gamma t\right)$.
- Equilibrium such that system is Schwarzchild stable (specific entropy increases outwards).
- Collisional (fluid) limit: magnetoviscous-thermal instability (MVTI).
- Collisionless limit: collisionless MTI.
- Estimated modal radial angular momentum fluxes $\langle T_{R\phi} \rangle$ and heat fluxes $\langle F_{ER} \rangle$ of instabilities:

$$\langle T_{R\phi} \rangle = \mathrm{Re}\left(\rho_0 \delta u_R \delta u_\phi^* - \frac{\delta B_R \delta B_\phi^*}{4\pi} + \delta\sigma_{\mathbf{bb}} \delta b_R^* \cos\chi \right),$$

$$\langle F_{ER} \rangle = \mathrm{Re}\left(\frac{5}{2}\rho_0 \delta\theta \delta u_R^* + \delta q \delta b_R^* - \frac{1}{3}\delta\sigma_{\mathbf{bb}} \delta b_R^* \right).$$

MHD Equations

Constituent MHD equations of continuity, force balance, thermal energy, and magnetic induction in a dilute plasma:

$$\left(\frac{\partial}{\partial t}+\Omega\frac{\partial}{\partial \phi}\right)\rho+\nabla\cdot(\rho\mathbf{u})=0,$$

$$\rho\left(\frac{\partial}{\partial t}+\Omega\frac{\partial}{\partial \phi}\right)\mathbf{u}+2\Omega\hat{\boldsymbol{z}}\times\rho\mathbf{u}+\Omega' R\rho u_R\hat{\boldsymbol{\phi}}=-\nabla\left(\frac{B^2}{8\pi}\right)+\frac{\mathbf{B}\cdot\nabla\mathbf{B}}{4\pi}+$$

$$\nabla\cdot\left(\sigma_{\mathbf{bb}}\left[\mathbf{bb}-\frac{1}{3}\mathbb{I}\right]\right)+\frac{\rho}{\rho_0}\nabla p_0,$$

$$\frac{3}{2}\left(\left[\frac{\partial}{\partial t}+\Omega\frac{\partial}{\partial \phi}\right]p+\nabla\cdot[p\mathbf{u}]\right)+p\nabla\cdot\mathbf{u}=\nabla\cdot(q\mathbf{b})+$$

$$\sigma_{\mathbf{bb}}\left(\mathbf{b}\cdot\nabla\mathbf{u}\cdot\mathbf{b}-\frac{1}{3}\nabla\cdot\mathbf{u}+\Omega' R b_R b_\phi\right),$$

$$\left(\frac{\partial}{\partial t}+\Omega\frac{\partial}{\partial \phi}\right)\mathbf{B}+\mathbf{u}\cdot\nabla\mathbf{B}=\mathbf{B}\cdot\nabla\mathbf{u}-\mathbf{B}\left(\nabla\cdot\mathbf{u}\right)+\Omega' R B_R\hat{\boldsymbol{\phi}}.$$

Forms of $\sigma_{\mathbf{bb}}$ and q whether *fluid* or *kinetic* analysis.

Analysis

- viscous stress and parallel heat flux are given by the following, where η_κ and η_ν are (electron) thermal and (ion) viscous diffusivities whose values are given by Braginskii (1965),

$$q = \frac{5}{2}\eta_\kappa \mathbf{b}\cdot(k_B T_e/m_e)\,,$$

$$\sigma_{\mathbf{bb}} = 3\rho\eta_\nu\left(\mathbf{b}\cdot\nabla\mathbf{u} - \frac{1}{3}\nabla\cdot\mathbf{u} + \Omega' R b_R \hat{\phi}\right).$$

- Fluid treatments applicable to regions where $T_i \simeq T_e$, therefore $\mathrm{Pr}^{-1} = \eta_\kappa/\eta_\nu = 101$.
- Analysis done in the incompressible limit – largely valid where $v_A \lesssim \theta_0^{1/2}$.

Dispersion Relation

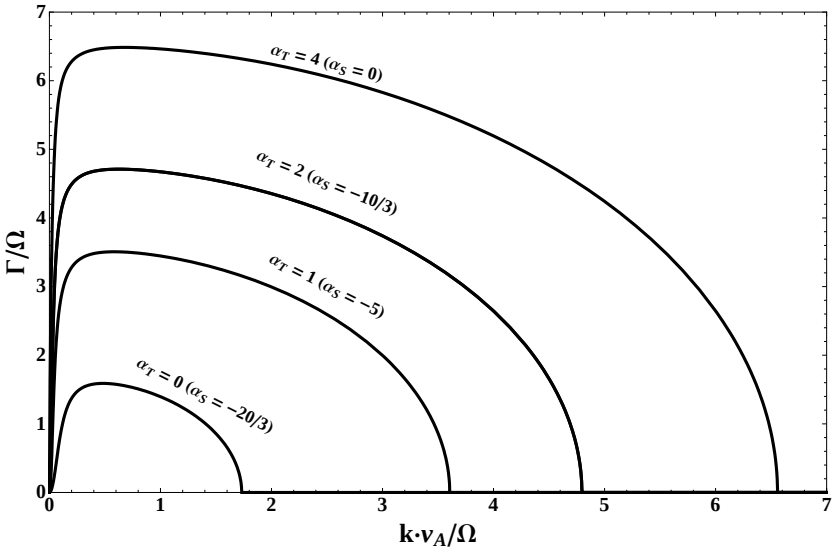

Plot of the growth rate as a function of wavenumber for various α_T for a Keplerian rotation profile and $\eta_\nu \Omega / v_A^2 = 10^2$.

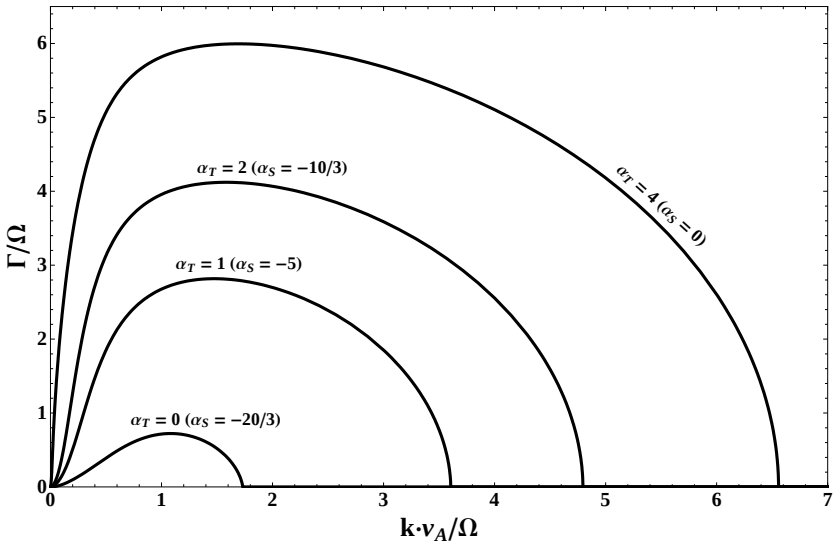

Plot of the dispersion relation for various α_T for a Keplerian rotation profile and a small viscous diffusion coefficient $\eta_\nu \Omega / v_A^2 = 1$.

Fluxes for MVI-Like Modes

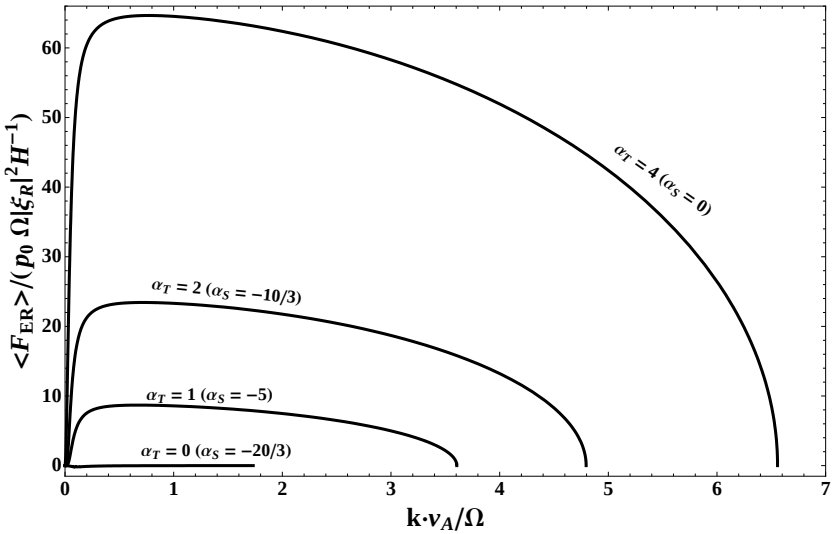

Normalized radial flux of thermal energy for a Keplerian rotational profile and $\eta_\nu \Omega / v_A^2 = 10^2$.

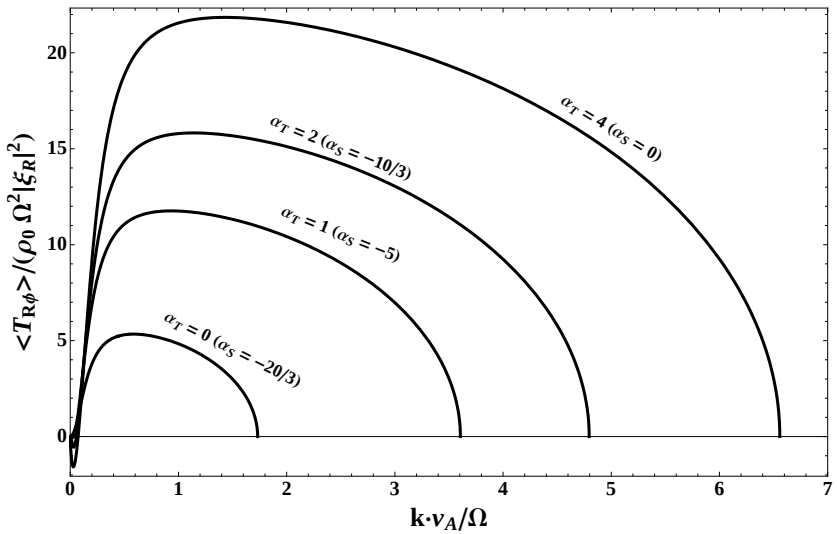

Normalized angular momentum flux for a Keplerian rotational profile and $\eta_\nu \Omega / v_A^2 = 10^2$.

Fluxes for MRI-Like Modes

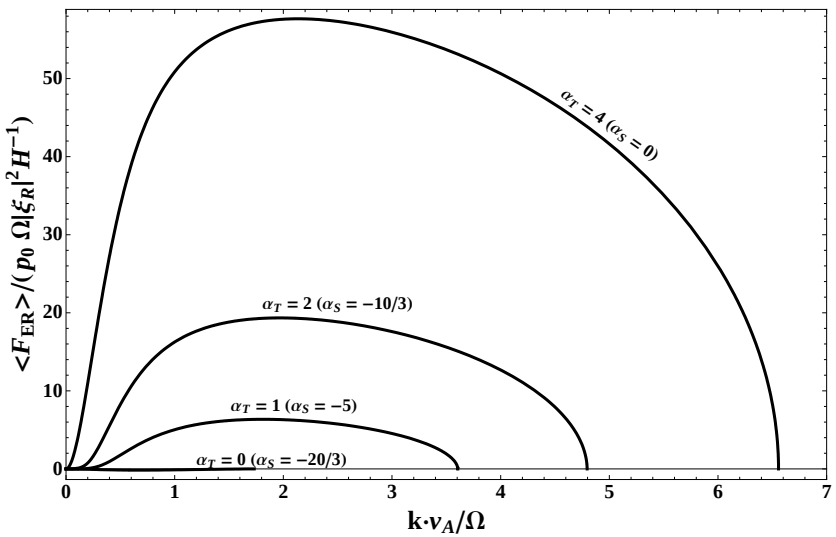

Normalized radial flux of thermal energy for a Keplerian rotational profile and $\eta_\nu \Omega / v_A^2 = 1$.

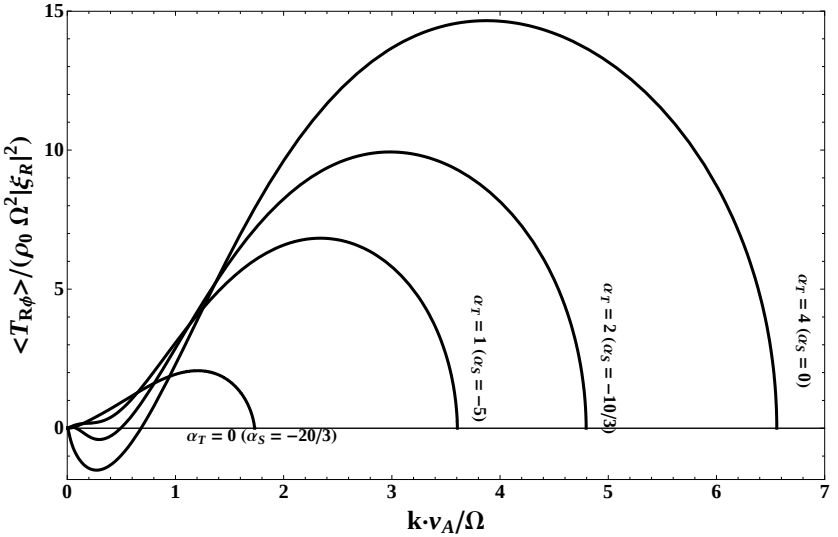

Normalized angular momentum flux for a Keplerian rotational profile and $\eta_\nu \Omega / v_A^2 = 1$.

Basics of Collisionless MHD in Rotating Frame

One works with the Boltzmann equation with, at most, mild collisionality,

$$\frac{\partial f}{\partial t} + \mathbf{U} \cdot \nabla f + \left(\mathbf{g} + \frac{Z_s e}{m_s} \left[\mathbf{E} + \frac{1}{c} \mathbf{U} \times \mathbf{B} \right] \right) \cdot \frac{\partial f}{\partial \mathbf{U}} = C[f]$$

Corotating, magnetic-field centered velocity transformation, $\mathbf{U} \rightarrow (v_{\parallel}, \mu, \psi)$:

$$v_{\parallel} = \mathbf{U} \cdot \mathbf{b} - R\Omega b_{\phi}$$

$$\mu = \frac{\left(\mathbf{U} - R\Omega\hat{\phi} + R\Omega b_{\phi}\mathbf{b} - \mathbf{b}\left(\mathbf{U} \cdot \mathbf{b}\right) - \mathbf{u}_{\perp} \right)^2}{2B},$$

$$\tan\psi = \frac{\hat{\mathbf{y}}_{\perp} \cdot \left(\mathbf{U} - R\Omega\hat{\phi} - \mathbf{u}_{\perp} \right)}{\hat{\mathbf{x}}_{\perp} \cdot \left(\mathbf{U} - R\Omega\hat{\phi} - \mathbf{u}_{\perp} \right)}.$$

After some algebra, and given our equilibrium, the lowest-order Boltzmann equation is the drift-kinetic equation (Kulsrud, 1983, 2005):

$$\left(\frac{\partial}{\partial t}+\Omega\frac{\partial}{\partial\phi}\right)f_s+\left(v_\parallel\mathbf{b}+\mathbf{u}_\perp\right)\cdot\nabla f_s+\left(\frac{Z_s eE_\parallel}{m_s}+\frac{m_p}{\rho_0 m_s}\mathbf{b}\cdot\nabla p_{s0}\right)\frac{\partial f_s}{\partial v_\parallel}+$$
$$\left(-\mathbf{b}\cdot\left(\left[\frac{\partial}{\partial t}+\Omega\frac{\partial}{\partial\phi}\right]\mathbf{u}_\perp+\left[\mathbf{u}_\perp+v_\parallel\mathbf{b}\right]\cdot\nabla\mathbf{u}_\perp\right)+\frac{1}{2}v_\perp^2\nabla\cdot\mathbf{b}\right)\frac{\partial f_s}{\partial v_\parallel}+$$
$$2\Omega\hat{\boldsymbol{z}}\cdot(\mathbf{b}\times\mathbf{u})-\Omega' R b_\phi\hat{\boldsymbol{R}}\cdot\left(\mathbf{u}_\perp+v_\parallel\mathbf{b}\right)\frac{\partial f_s}{\partial v_\parallel}=C\left[f_s\right].$$

Parallel and perpendicular pressures to the magnetic field, $p_\parallel$ and $p_\perp$,

$$p=\tfrac{2}{3}p_\perp+\tfrac{1}{3}p_\parallel,\qquad \sigma_{\mathbf{bb}}=p_\parallel-p_\perp,$$
$$p_{s\parallel}=2\pi m_s\int f_s v_\parallel^2\,dv_\parallel\,v_\perp\,dv_\perp,\quad p_{s\perp}=2\pi m_s\int f_s\left(\frac{1}{2}v_\perp^2\right)\,dv_\parallel\,v_\perp\,dv_\perp.$$

Dispersion Relation

At high β, collisionless MTI appears qualitatively similar to MVTI. Below are plots of the dispersion relation for $\beta = 10^2$, $\chi = \pi/4$, $\alpha_P = 5$, and $0 \leq \alpha_T \leq 2$.

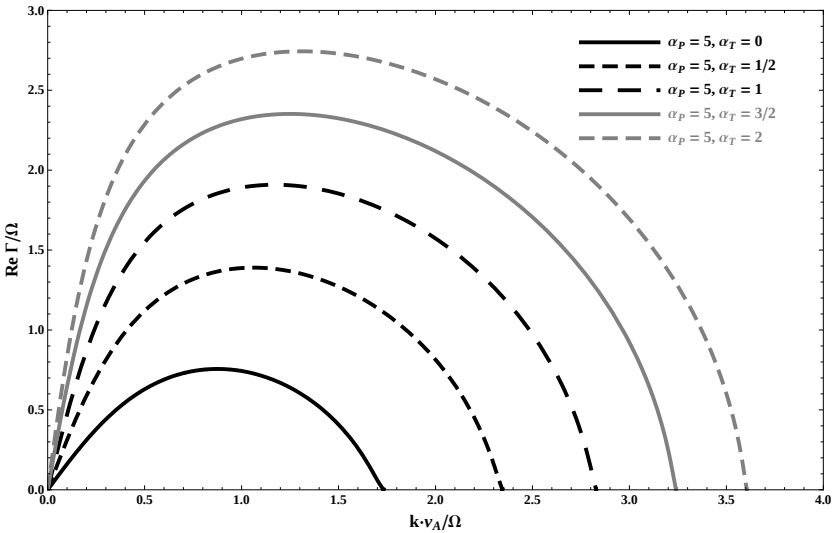

The real part of the growth rate for the collisionless MTI with various equilibrium temperature and pressure profiles.

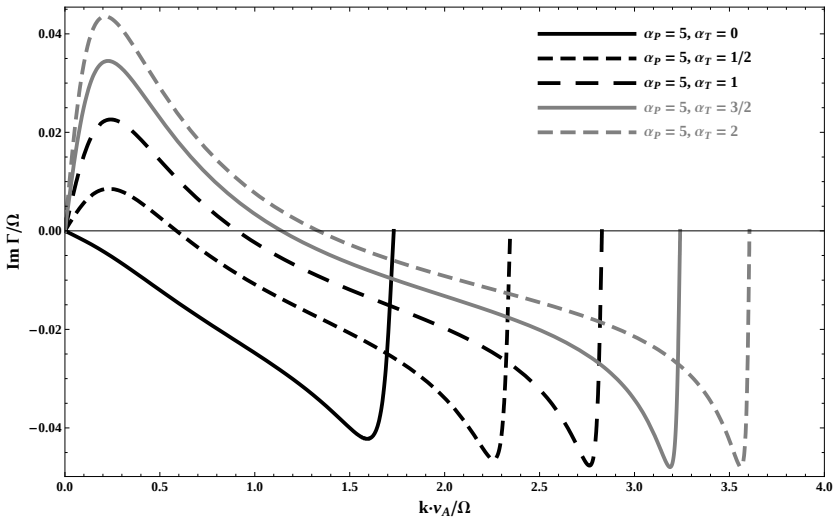

The imaginary part of the growth rate for the collisionless MTI with various equilibrium temperature and pressure profiles.

Dispersion Relation

Collisionless damping of long wavelength modes $k_{||} < \Omega/v_i$ (see, e.g., Quataert et al. (2002); Sharma et al. (2003)). As $\beta \rightarrow 1$, anisotropic pressure becomes dynamically unimportant.

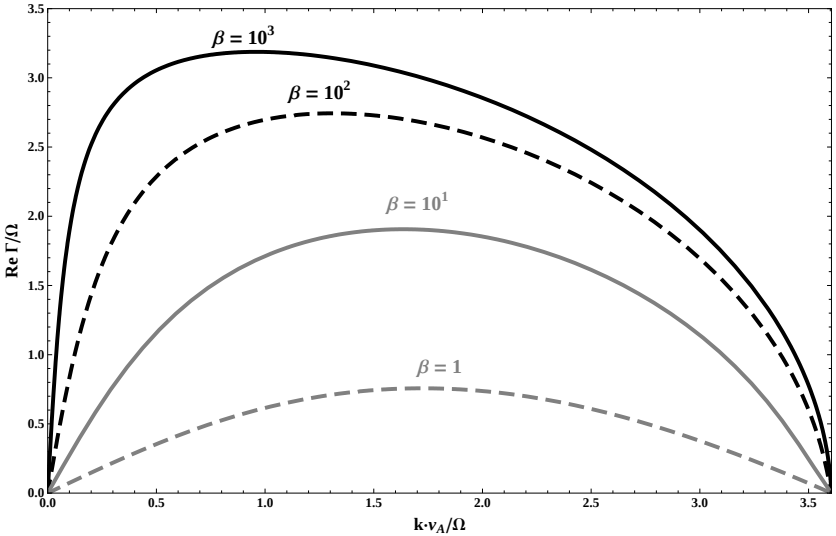

The real component of the growth rate for various β, $\chi = \pi/4$, $\alpha_{\boldsymbol{P}} = 5$, and $\alpha_{\boldsymbol{T}} = 2$. For large β we reproduce MRI-like modes.

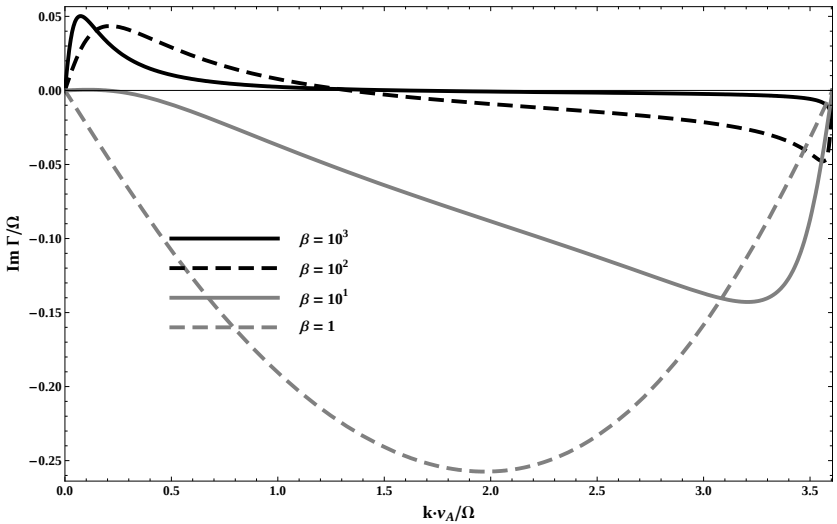

The imaginary component of the growth rate for various β, $\chi = \pi/4$, $\alpha_{\boldsymbol{P}} = 5$, and $\alpha_{\boldsymbol{T}} = 2$. For large β the imaginary component reaches a maximum where the growth rate reaches a maximum. As $\beta \rightarrow 1$, the imaginary component of the growth rate increases in magnitude.

Modal Fluxes

Modal fluxes $\langle F_{ER} \rangle$ and $\langle T_{R\phi} \rangle$ for a Keplerian-like rotation profile, $\beta = 10^2$, and $\chi = \pi/4$, $\alpha_P = 5$, and $0 \leq \alpha_T \leq 2$.

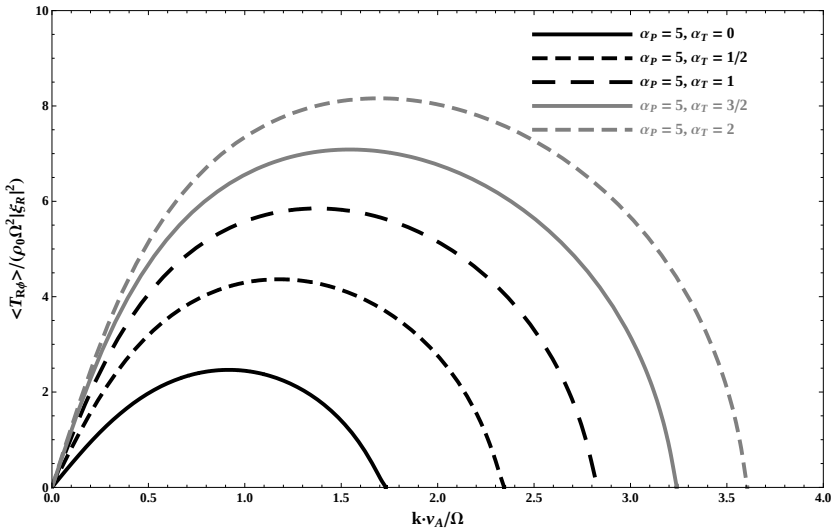

Normalized angular momentum flux for collisionless MTI.

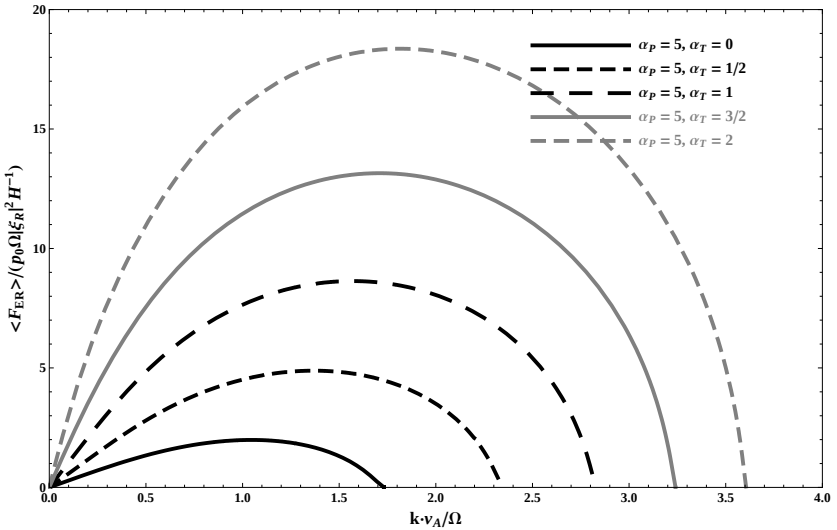

Normalized heat flux for collisionless MTI.

Mildly Collisional MTI

In the limit that mean free path is larger than wavelength of fastest growing modes, i.e., $\nu \gtrsim \Omega\beta^{1/2}$, we reproduce the MVTI (see, e.g., Sharma et al. (2003)).

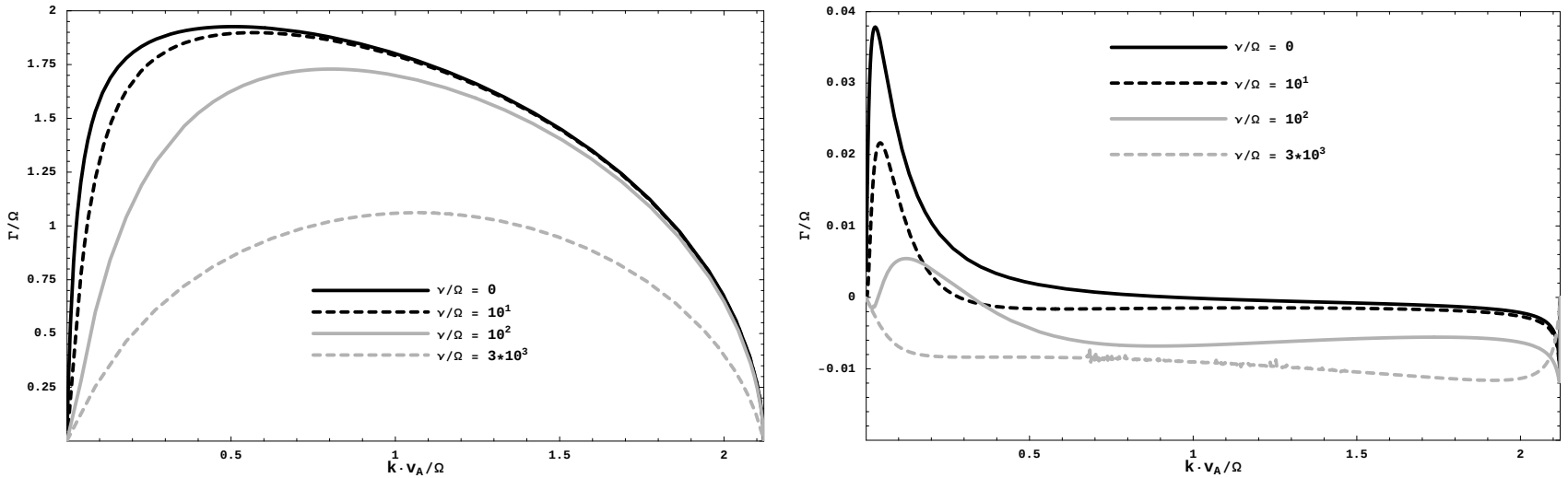

Real (left) and imaginary (right) parts of the growth rate of the MVTI. We reproduce the MVTI dispersion relation for $\nu_i \geq \Omega\beta^{1/2}$.

Finite Electron Temperature Effects

Not significant different in growth rates if we include electron thermal dynamics in the dispersion relation.

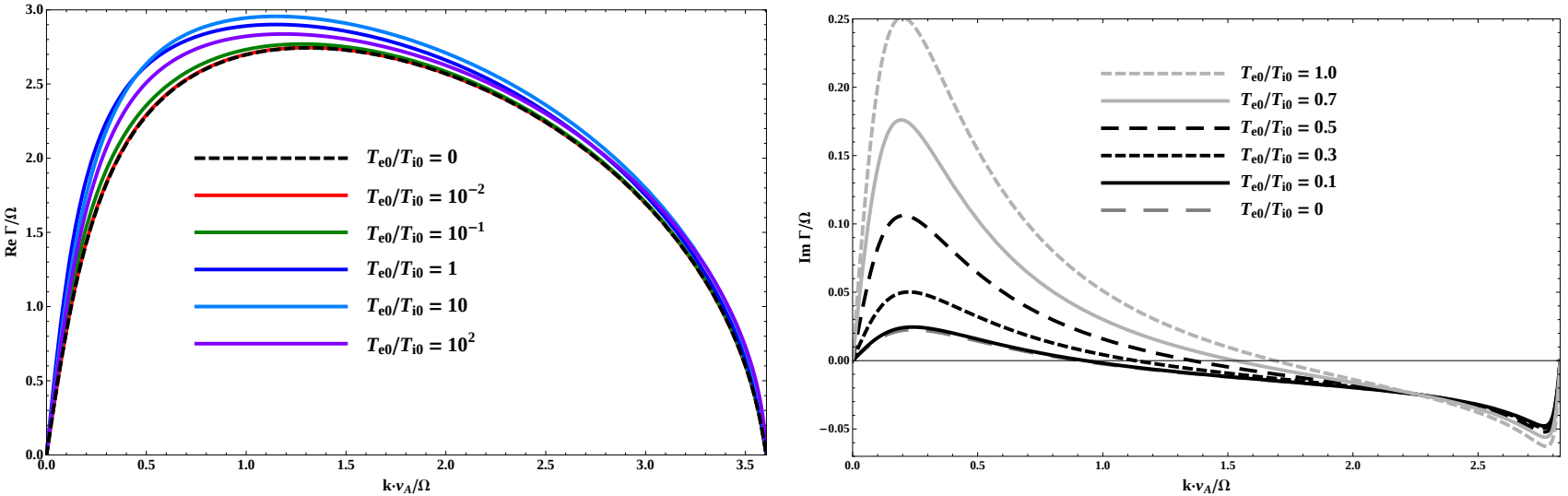

The real (left) and imaginary (right) parts of growth rate of the collisionless MTI. The imaginary part of the growth rates where $T_{e0}/T_{i0} = 10^{-1}$ nearly coincide where $T_{e0}/T_{i0} = 0$.

Off-Plane Collisionless MHD Effects

We take $\beta = 10^2$. At left is the real, and at right is the imaginary, normalized growth rate as a function of height z/H for $k_Z v_{A0}/\Omega = 10^{-1}$. We compare Γ to a simplified growth rate, Γ_s, where effects due to equilibrium acceleration are ignored.

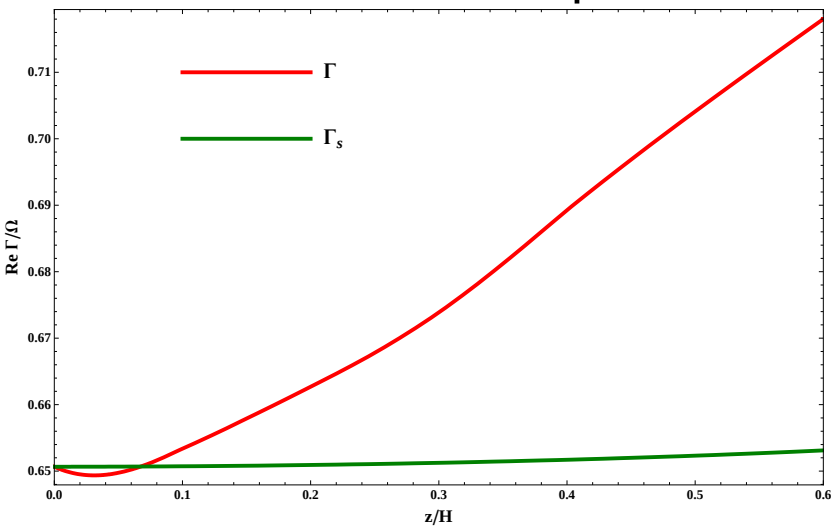

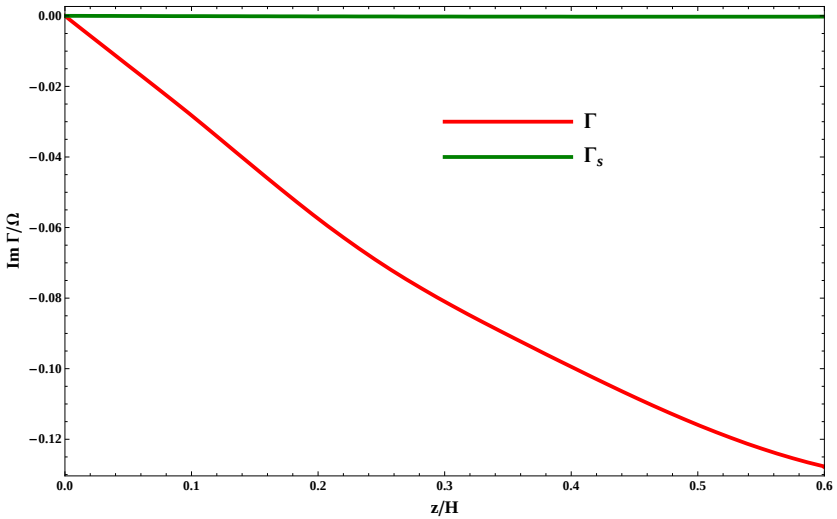

Improved Landau Fluid Closures Necessary

Standard forms of heat fluxes in a collisionless MHD plasma (Snyder et al., 1997):

$$\frac{\delta q_{\parallel}}{p_{i0} v_i} = 2i\sqrt{\frac{2}{\pi}}\left(\frac{\delta\rho}{\rho_0} - \frac{\delta p_{\parallel}}{p_{i0}}\right) - 2\left(\frac{1}{k_{\parallel}}\frac{\partial \ln T_0}{\partial R}\right)\sqrt{\frac{2}{\pi}}\frac{\delta B_R}{B_0}$$

$$\frac{\delta q_{\perp}}{p_{i0} v_i} = i\sqrt{\frac{2}{\pi}}\left(\frac{\delta\rho}{\rho_0} - \frac{\delta p_{\perp}}{p_{i0}}\right) - \left(\frac{1}{k_{\parallel}}\frac{\partial \ln T_0}{\partial R}\right)\sqrt{\frac{2}{\pi}}\frac{\delta B_R}{B_0}$$

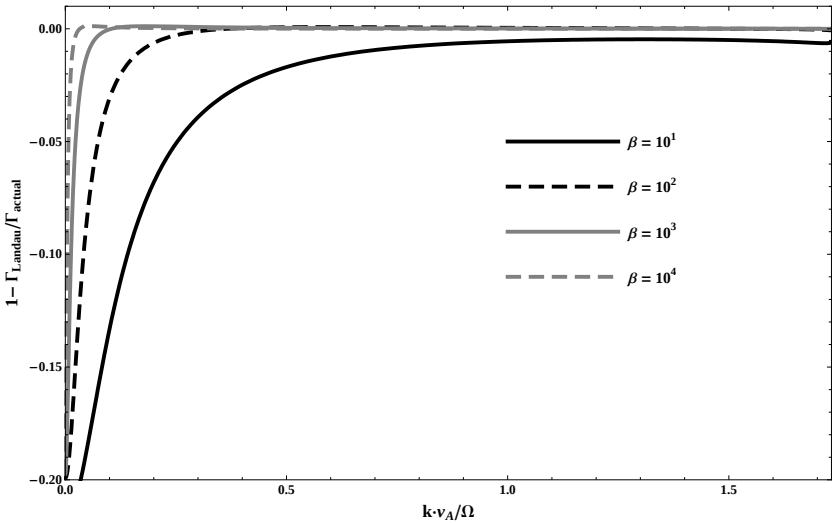

Collisionless MRI

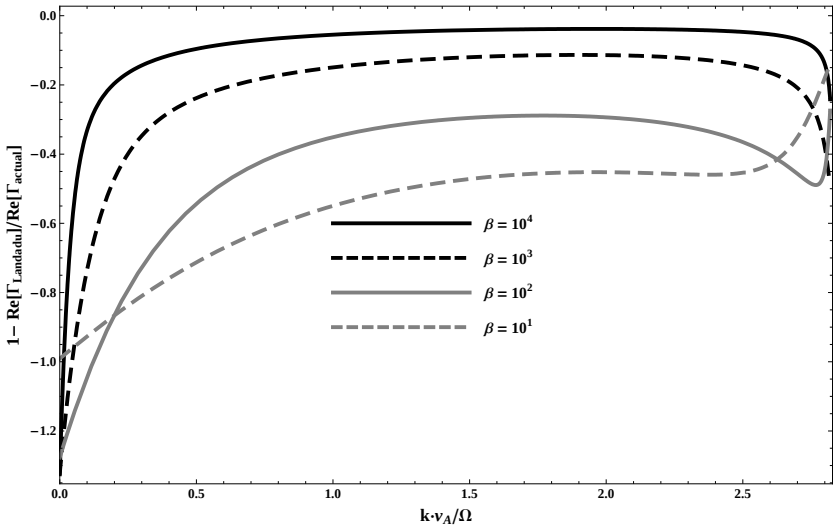

Collisionless MTI

Isotropizing Gyrokinetic Instabilities

- Treatment of firehose and mirror instabilities considered as a "hard wall" on pressure anisotropy by Sharma et al. (2006); Sharma (2006); Sharma et al. (2007) for collisionless MRI.
- Treatments of collisionless turbulence (Schekochihin & Cowley, 2005; Howes et al., 2007a,b) may need to address this in order to accurately describe dynamics of collisionless MHD plasmas.

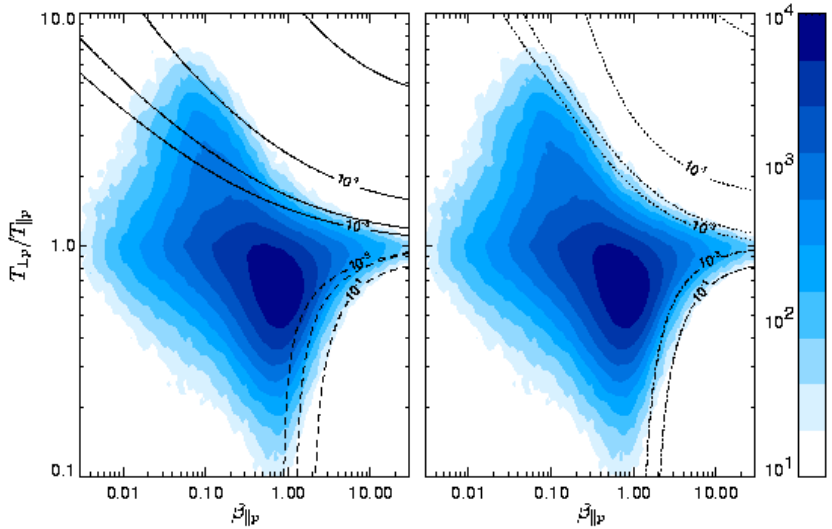

Density histogram of measurements of the solar wind by the WIND telescope. Fits of histogram to threshold instability to cyclotron and mirror instabilities, as determined by particle simulations of Gary et al. (1996, 1997). This figure is taken from Hellinger et al. (2006).

Necessity of Global Simulations

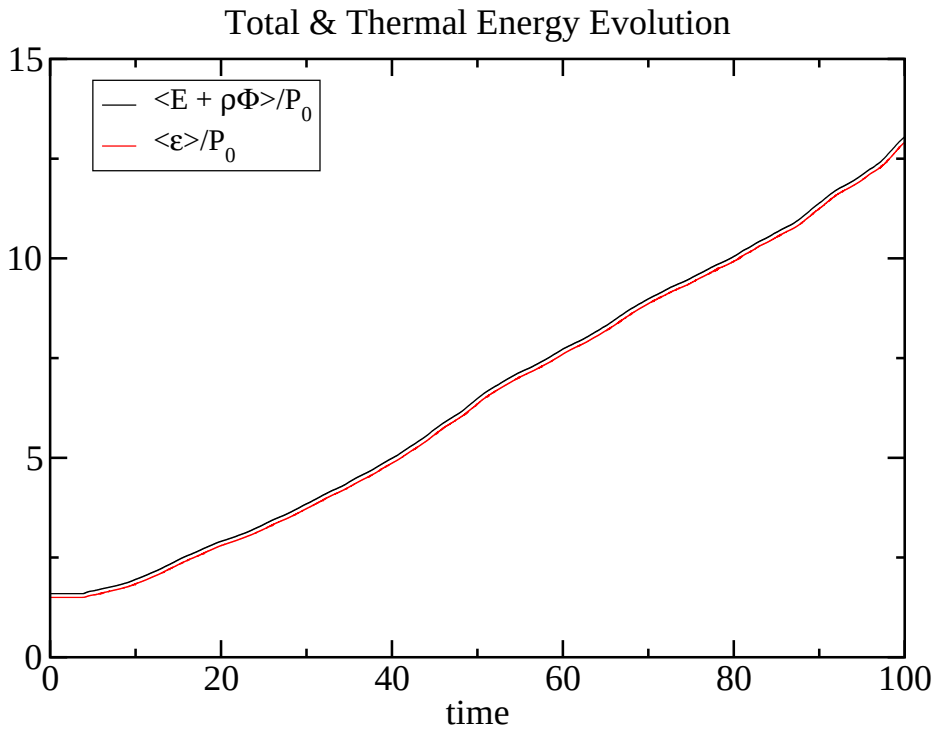

Secular increase of total energy within a radial slice for simulation of the MRI. Figure taken from Gardiner & Stone (2005).

Global simulations are **necessary** for modeling radiatively inefficient flows; codes that explicitly conserve all energy, such as Athena (Gardiner & Stone, 2005), are necessary to model the nonlinear collisionless MTI or MVTI.

Main Points

- Both collisionless MTI and MVTI can provide significant outward heat and angular momentum fluxes to drive accretion in radiatively inefficient flows.
- Decreasing β (increasing relative strength of magnetic field) results in decreased anisotropic fluxes of heat and momentum in linear collisionless MTI.
- Simplified analysis (neglect of electron temperature) is valid in case where $T_i \gtrsim T_e$; further work needed to characterize the effects of finite equilibrium acceleration in collisionless off-plane MTI.

References

Baganoff, F. K., Maeda, Y., Morris, M., Bautz, M. W., Brandt, W. N., Cui, W., Doty, J. P., Feigelson, E. D., Garmire, G. P., Pravdo, S. H., Ricker, G. R., & Townsley, L. K. 2003, ApJ, 591, 891

Balbus, S. A. 2001, ApJ, 562, 909

—. 2004a, ApJ, 600, 865

—. 2004b, ApJ, 616, 857

Balbus, S. A. & Hawley, J. F. 1991, ApJ, 376, 214

Balbus, S. A., Hawley, J. F., & Stone, J. M. 1996, ApJ, 467, 76

Beckert, T., Duschl, W. J., Mezger, P. G., & Zylka, R. 1996, A&A, 307, 450

Bower, G. C., Wright, M. C. H., Falcke, H., & Backer, D. C. 2003, ApJ, 588, 331

Braginskii, S. I. Reviews of Plasma Physics, Vol. 1 (New York: Consultants Bureau), 205–311

Chandrasekhar, S. 1960, Proceedings of the National Academy of Science, 46, 253

De Villiers, J.-P., Hawley, J. F., & Krolik, J. H. 2003, ApJ, 599, 1238

Di Matteo, T., Allen, S. W., Fabian, A. C., Wilson, A. S., & Young, A. J. 2003, ApJ, 582, 133

Francis, P. J., Hewett, P. C., Foltz, C. B., Chaffee, F. H., Weymann, R. J., & Morris, S. L. 1991, ApJ, 373, 465

Frank, J., King, A., & Raine, D. 2002, Accretion Power in Astrophysics (Cambridge: Cambridge University Press), 93

Gardiner, T. & Stone, J. 2005, J. Comp. Phys., 205, 509

Gary, S. P., McKean, M. E., & Winske, D. 1996, Geophys. Res. Lett., 23, 2887

Gary, S. P., Wang, J., Winske, D., & Fuselier, S. A. 1997, J. Geophys. Res., 102, 27159

Ghez, A. M., Becklin, E., Duchjne, G., Hornstein, S., Morris, M., Salim, S., & Tanner, A. 2003, Astronomische Nachrichten Supplement, 324, 527

Hawley, J. F., Balbus, S. A., & Stone, J. M. 2001, ApJ, 552, L49

Hawley, J. F., Balbus, S. A., & Winters, W. F. 1998, ApJ, 440, 372

Hawley, J. F., Gammie, C. F., & Balbus, S. A. 1996, ApJ, 464, 690

Hellinger, P., Trvnek, P., Kasper, J. C., & Lazarus, A. J. 2006, Geophys. Res. Lett., 33, 9101

Ho, L. C., Terashima, Y., & Ulvestad, J. S. 2003, ApJ, 589, 783

Howes, G. G., Cowley, S. C., Dorland, W., Hammett, G., Quataert, E., & Schekochihin, A. A. 2007a, in American Astronomical Society Meeting Abstracts, Vol. 210, American Astronomical Society Meeting Abstracts

Howes, G. G., Cowley, S. C., Dorland, W., Hammett, G. W., Quataert, E., & Schekochihin, A. A. 2007b, ArXiv e-prints, 707

Islam, T. S. & Balbus, S. A. 2005, ApJ, 633, 328

Ji, H., Burin, M., Schartman, E., & Goodman, J. 2006, Nature, 444, 343

Kulsrud, R. M. 1983, in Basic Plasma Physics: Selected Chapters, Handbook of Plasma Physics, Volume 1, ed. A. A. Galeev & R. N. Sudan, 1–115

Kulsrud, R. M. 2005, Plasma Physics for Astrophysics (Princeton, N.J.: Princeton University Press)

Lesur, G. & Longaretti, P.-Y. 2005, A&A, 444, 25

Loewenstein, M., Mushotzky, R. F., Angelini, L., Arnaud, K. A., & Quataert, E. 2001, apjl, 555, L21

Lynden-Bell, D. 1969, Nature, 223, 690

Menou, K. 2005, in KITP Program: Physics of Astrophysical Outflows and Accretion Disks

Narayan, R. 2002, in Lighthouses of the Universe: The Most Luminous Celestial Objects and Their Use for Cosmology Proceedings of the MPA/ESO, 405

Narayan, R., Mahadevan, R., Grindlay, J. E., Popham, R. G., & Gammie, C. 1998, ApJ, 492, 554

Quataert, E., Dorland, W., & Hammett, G. W. 2002, ApJ, 577, 524

Richstone, D., Ajhar, E. A., Bender, R., Bower, G., Dressler, A., Faber, S. M., Filippenko, A. V., Gebhardt, K., Green, R., Ho, L. C., Kormendy, J., Lauer, T. R., Magorrian, J., & Tremaine, S. 1998, Nature, 395, A14+

Schekochihin, A. A. & Cowley, S. C. 2005, ArXiv Astrophysics e-prints

Schdel, R., Ott, T., Genzel, R., Hofmann, R., Lehnert, M., Eckart, A., Mouawad, N., Alexander, T., Reid, M. J., Lenzen, R., Hartung, M., Lacombe, F., Rouan, D., Gendron, E., Rousset, G., Lagrange, A.-M., Brandner, W., Ageorges, N., Lidman, C., Moorwood, A. F. M., Spyromilio, J., Hubin, N., & Menten, K. M. 2002, Nature, 419, 694

Sharma, P. 2006, PhD thesis, Princeton University

Sharma, P., Hammett, G. W., & Quataert, E. 2003, ApJ, 596, 1121

Sharma, P., Hammett, G. W., Quataert, E., & Stone, J. 2006, ApJ, 637, 952

Sharma, P., Quataert, E., Hammett, G. W., & Stone, J. M. 2007, ApJ, 667, 714

Snyder, P. B., Hammett, G. W., & Dorland, W. 1997, Phys. Plasmas, 4, 11

Velikhov, E. P. 1959, Sov. Phys. JETP, 9, 995

Winter, L. M., Mushotzky, R. F., Tueller, J., Reynolds, C. S., & Markwardt, C. 2007, in American Astronomical Society Meeting Abstracts, Vol. 210, American Astronomical Society Meeting Abstracts